Science Advances
AAAS

advances.sciencemag.org/cgi/content/full/6/3/eaay6200/DC1

Supplementary Materials for

Picosecond-resolution phase-sensitive imaging of transparent objects in a single shot

Taewoo Kim, Jinyang Liang, Liren Zhu, Lihong V. Wang*

*Corresponding author. Email: lvw@caltech.edu

Published 17 January 2020, *Sci. Adv.* **6**, eaay6200 (2020)
DOI: 10.1126/sciadv.aay6200

The PDF file includes:

Other Supplementary Material for this manuscript includes the following:

(available at advances.sciencemag.org/cgi/content/full/6/3/eaay6200/DC1)

Section S1. Dark-field intensity as a function of the phase

Here, we derive the dark-field intensity as a function of the phase delay $\phi(x, y; t)$ added by the transparent object to be imaged, where x and y denote the transverse Cartesian coordinates (Fig. 1) and t denotes time. Let us start with a pulsed incident plane wave, with field $U_0(x, y; t)$. Even though a plane wave does not have *x* and *y* dependence, we write *x* and *y* explicitly for readability and potential generalization. If attenuation is negligible, the transmitted field immediately after the phase object is given by $U_t(x, y; t) = U_0(x, y; t) \exp(i\phi(x, y; t))$. For a small on-axis beam block placed on the Fourier plane of the dark-field system, the transfer function, $H(k_x, k_y)$, can be defined as $H(k_x, k_y) = 0$ near $k_x = 0, k_y = 0$, and 1 elsewhere. The field after the beam block in the spatial frequency domain is

$$\widetilde{U}_{df}(k_x, k_y; t) = \widetilde{U}_t(k_x, k_y; t)H(k_x, k_y) \tag{S1}$$

where $\widetilde{U}_t(k_x, k_y; t)$ is the 2D spatial Fourier transform of $U_t(x, y; t)$.

The phase function can be expanded to $\phi(x, y; t) = \phi_0(t) + \phi_1(x, y; t)$, where ϕ_0 denotes the spatially averaged phase and ϕ_1 denotes the spatial variation. Therefore, the transmitted field can be decomposed to

$$U_t(x, y; t) = U_{t0}(x, y; t) + U_{t1}(x, y; t) \tag{S2}$$

where $U_{t0}(x, y; t) = U_0(x, y; t) \exp(i\phi_0(t))$ represents the unscattered field, and $U_{t1}(x, y; t) = U_0(x, y; t) \exp(i\phi_1(x, y; t))$ represents the scattered field. The spatial Fourier transform counterpart of Eq. (S2) is

$$\widetilde{U}_t(k_x, k_y; t) = \widetilde{U}_{t0}(k_x, k_y; t) + \widetilde{U}_{t1}(k_x, k_y; t) \tag{S3}$$

By inserting Eq. (S3), the right-hand side of Eq. (S1) becomes

$$\widetilde{U}_t(k_x, k_y; t)H(k_x, k_y) = \widetilde{U}_{t0}(k_x, k_y; t)H(k_x, k_y) + \widetilde{U}_{t1}(k_x, k_y; t)H(k_x, k_y) \tag{S4}$$

For a planar incident wave, the DC component —i.e., the unscattered field— is completely blocked: $\widetilde{U}_{t0}(k_x, k_y; t)H(k_x, k_y) = 0$. If $\widetilde{U}_{t1}(k_x, k_y; t)$ has a broad spatial spectrum, the beam block's effect is negligible: $\widetilde{U}_{t1}(k_x, k_y; t)H(k_x, k_y) = \widetilde{U}_{t1}(k_x, k_y; t)$. Therefore, Eq. (S4) becomes $\widetilde{U}_t(k_x, k_y; t)H(k_x, k_y) = \widetilde{U}_{t1}(k_x, k_y; t)$. Consequently, Eq. (S1) becomes

$$\widetilde{U}_{df}(k_x, k_y; t) = \widetilde{U}_{t1}(k_x, k_y; t) \tag{S5}$$

as expected for dark-field imaging, which captures only the scattered field. Merging Eq. (S3) and (S5) yields

$$\widetilde{U}_{df}(k_x, k_y; t) = \widetilde{U}_t(k_x, k_y; t) - \widetilde{U}_{t0}(k_x, k_y; t) \tag{S6}$$

Transforming Eq. (S6) back to the spatial domain, we obtain

$$\begin{aligned} U_{df}(x, y; t) &= U_0(x, y; t)\exp\big(i\phi_0(t) + i\phi_1(x, y; t)\big) - U_0(x, y; t)\exp\big(i\phi_0(t)\big) \\ &= U_0(x, y; t)\exp\big(i\phi_0(t)\big)\big[\exp\big(i\phi_1(x, y; t)\big) - 1\big] \end{aligned} \tag{S7}$$

Equation (S7) defines the imaged field, which can be converted to a phase-dependent intensity function

$$\begin{aligned} I_{df}(x,y;t) &= \left|U_{df}(x,y;t)\right|^2 \\ &= I_0(x,y;t)\left|\exp\left(i\phi_1(x,y;t)\right)-1\right|^2 \\ &= 2I_0(x,y;t)(1-\cos\phi_1(x,y;t)) \end{aligned} \tag{S8}$$

where $I_0(x,y;t) = |U_0(x,y;t)|^2$. When the object does not have any spatial variations—i.e., $\phi_1(x,y;t) = 0$, $I_{df}(x,y;t)$ becomes 0, as expected in dark-field imaging.

The main purpose of this derivation is to prove that the source of the intensity distribution obtained from dark-field imaging measures the phase delay. This derivation is inapplicable to strongly scattering objects.

Section S2. SBR and SNR analysis for various beam block sizes

In pCUP, it is important to minimize the background of the dark-field image because the background overlaps with the phase signal in time-sheared raw images and reduces the contrast. Therefore, the beam block diameter needs to be optimized to maximize SBR and SNR in the dark-field images. In practice, the beam block size is greater than the theoretical focal point size, because of the imperfect incident plane wave and the aberrations in the imaging system.

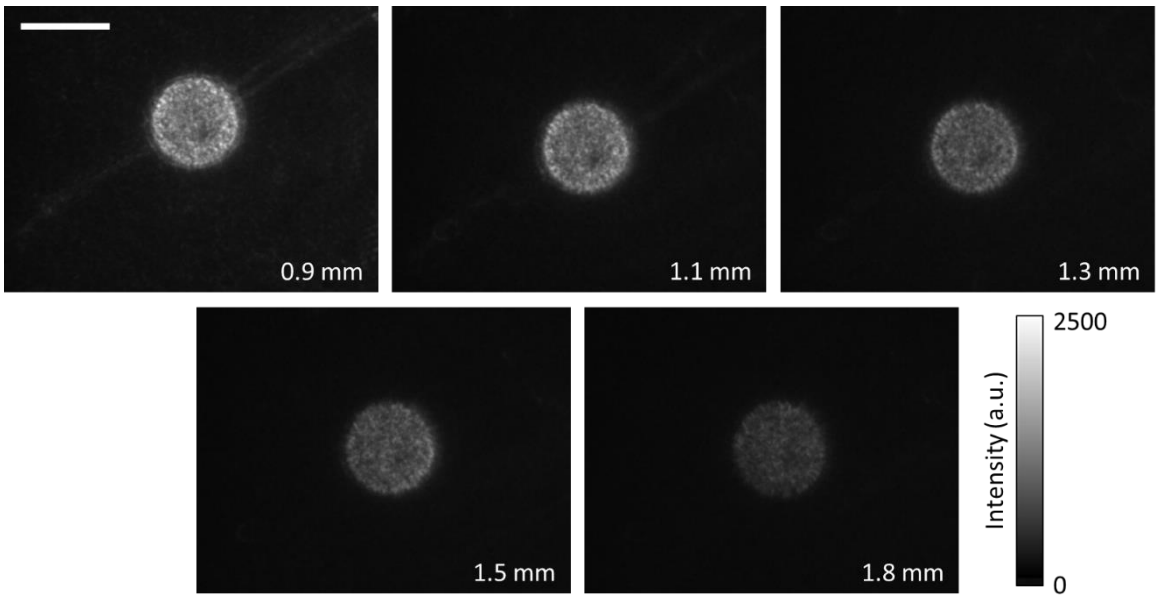

Fig. S1. Dark-field images of a 50-µm-diameter polystyrene bead in water with various beam block diameters.

In order to optimize the SBR and the SNR, we imaged a 50-µm-diameter polystyrene bead in water for various beam block sizes. Figure S1 shows five images of the same field of view, imaged with beam block diameters varying from 0.9 mm to 1.8 mm. As the block becomes larger, not only does the background intensity reduce, but also the signal intensity from the bead reduces.

Table S1 shows the SBR and SNR measured with each beam block. We measured the SBR by dividing the average signal inside the bead by the average signal of the background. We also measured the SNR by dividing the average signal inside the bead by the standard deviation inside the bead. For our imaging system using a 20× objective lens, the beam block with a 1.1 mm diameter provided the highest SBR and SNR. For the 1× imaging system used for the Kerr effect measurement, the beam block with a 1.8 mm diameter was used.

Table S1. SBR and SNR for various beam block diameters with a 20× objective.

Diameter (mm)	SBR	SNR
0.9	5.79	8.86
1.1	6.70	13.4
1.3	5.06	10.5
1.5	5.04	9.84
1.8	3.82	7.38

Section S3. Improved lossless encoding by the dove prisms

As shown in Fig. 1, two dove prisms are inserted to the LLE-CUP system in order to further improve the encoding and reconstruction. By adding the dove prisms, the two complementary views experience shearing in opposite directions. This modification improved the reconstruction of the expanding shockwave by allowing for a reduced overlap of the phase signals. Figure S2 illustrates the raw pCUP image formation for upright and 180° rotated cases. The raw pCUP image is a summation of all frames with a time dependent shearing along the *y*-axis. For each frame, the radius of the shockwave increases, and the center of the shockwave moves downwards. Therefore, the phase signal from the top half of the shockwave experiences spatial overlap in the raw image, while the bottom half of the shockwave is spread out in the raw image. As a result, the top half of the shockwave is less sparse for reconstruction.

Without the dove prisms, both of the complementary views, sheared in the same direction, lack sparsity in the top half of the shockwave. By adding the dove prisms to rotate the second view 180° while matching the path lengths, the bottom half of the shockwave is located at the top of the image in the second view. Therefore, the raw image from the second view shows an overlapped bottom half of the shockwave and a spread top half of the shockwave. This rotated

second view reduces the reconstruction ambiguity in the top half of the shockwave and allows for a more robust reconstruction of the shockwave.

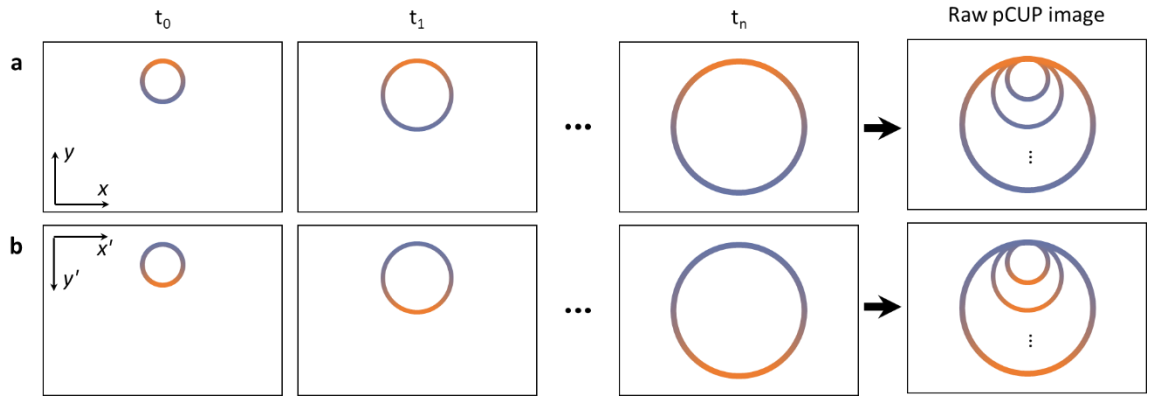

Fig. S2. Illustration of the raw image formation with 180° rotated complementary views. (**a**) The original pCUP raw image formation without a 180° rotation. The signals from the top half of the shockwave (shown in orange) are overlapped in the raw image. (**b**) The raw image formation with a 180° rotation. The bottom half (shown in blue) is placed at the top of the image and experiences the overlap of signals.